Experimental and kinetic modeling study of extinction and ignition of methyl decanoate in laminar non-premixed flows

Kalyanasundaram Seshadri, Tianfeng Lu, Olivier Herbinet, Stefan Humer, Ulrich Niemann, William J. Pitz, Reinhard Seiser, Chung K. Law

Experimental and kinetic modeling study of extinction and ignition of methyl decanoate in laminar non-premixed flows

Kalyanasundaram Seshadri[1], Tianfeng Lu[2], Olivier Herbinet[3], Stefan Humer[1], Ulrich Niemann[1], William J. Pitz[3], Reinhard Seiser[1], Chung K. Law[2]

[1] Department of Mechanical and Aerospace Engineering, University of California at San Diego, 9500 Gilman Drive, Mail Code 0411, La Jolla, CA 92093-0411, USA
[2] Department of Mechanical and Aerospace Engineering, Princeton University, Princeton, NJ 08544, USA
[3] Lawrence Livermore National Laboratory, Livermore, CA 94550, USA

Abstract

Methyl decanoate is a large methyl ester that can be used as a surrogate for biodiesel. In this experimental and computational study, the combustion of methyl decanoate was investigated in non-premixed, nonuniform flows. Experiments were performed employing the counterflow configuration with a fuel stream made up of vaporized methyl decanoate and nitrogen, and an oxidizer stream of air. The mass fraction of fuel in the fuel stream was measured as a function of the strain rate at extinction, and critical conditions of ignition were measured in terms of the temperature of the oxidizer stream as a function of the strain rate. A detailed mechanism of 8555 elementary reactions and 3036 species has been developed previously to describe combustion of methyl decanoate. Since it is not possible to use this detailed mechanism to simulate the counterflow flames because the number of species and reactions is too large to employ with current flame codes and computer resources, a skeletal mechanism was deduced from this detailed mechanism using the "directed relation graph" method. This skeletal mechanism has only 713 elementary reactions and 125 species. Critical conditions of extinction and critical conditions of ignition were calculated using this skeletal mechanism and they were found to agree well with experimental data. In general, the methyl decanoate mechanism provides a realistic kinetic tool for simulation of biodiesel fuels.

Keywords: Biodiesel; Methyl decanoate; Surrogate; Non premixed; Chemical-kinetic mechanism

1. Introduction

There is considerable interest in understanding the combustion of biodiesel because it is recognized as an alternative and renewable fuel. Methyl esters, in particular methyl butanoate (*n*-$C_3H_7C(=O)OCH_3$) and methyl decanoate (n-$C_9H_{19}C(=O)OCH_3$), have been proposed as possible surrogates for biodiesel [1-7]. Kinetic modeling of methyl butanoate has concluded that this fuel reproduces kinetic features of the oxidation of the methyl ester, but does a poor job of reproducing kinetic features of diesel fuels with their chains of 16–18 carbon atoms. Other studies have used kinetic models for normal alkanes as large as *n*-hexadecane to simulate the combustion of the large methyl ester molecules in actual biodiesel fuels. Recently Herbinet et. al. [7] developed a reliable kinetic model for describing the combustion of methyl decanoate, which has a chain of 10 carbon atoms with a methyl ester group attached. Methyl decanoate reacts in a manner that is much closer to actual biodiesel fuel than methyl butanoate, including both early production of CO_2 from the methyl ester group and burning in a manner very similar to biodiesel derived from rapeseed-based methyl esters.

Previous studies of ignition and combustion of methyl decanoate have been focused on premixed systems [5-7]. The present study considers combustion of methyl decanoate in non-premixed, aerodynamically strained flows. It is important to examine combustion characteristics and validate chemical-kinetic models under conditions of fluid dynamic strain because these conditions are often found in practical combustion situations such as those within internal combustion engines where there are high rates of swirl. Extinction characteristics are examined because flame extinction in high strained flows is an important problem in gas turbine engines. Ignition under aerodynamic strain is relevant because fuel/air mixtures must be ignited in flows in internal combustion engines under these conditions. Experiments were carried out employing the counterflow configuration. Critical conditions of extinction and ignition were measured. The chemical-kinetic mechanism for methyl decanoate was tested by comparing predictions of this mechanism with experimental data.

2. Experimental apparatus and procedures

Figure 1 shows a schematic illustration of the counterflow system. Prevaporized fuel mixed with nitrogen is injected from the fuel-duct, and a stream of air is injected from the oxidizer-duct. The exit of the fuel-duct is called the fuel boundary, and the exit of the oxidizer-duct the oxidizer boundary. The inner diameter of the fuel-duct is 23.1 mm and the inner diameter of the oxidizer-duct is 22.3 mm. Silicon-carbide heating elements are placed inside the oxidizer-duct to heat the air for the ignition experiments. The level of electrical heating to these elements is controlled using a variable transformer. The temperature of the fuel stream and the temperature of the oxidizer stream at the boundaries are measured using thermocouples. The temperatures are corrected for radiation losses. Liquid fuel and nitrogen are introduced into an electrically heated vaporizer that is maintained at a constant temperature. The volumetric flow rate of the liquid into the vaporizer is measured using a syringe pump. The temperature inside the vaporizer is monitored by a thermocouple. The vaporizer temperature is maintained at 478 K. The nitrogen is introduced into the vaporizer at a pressure and temperature that is nearly equal to atmospheric pressure and temperature. The flow rates of gases are adjusted by computer-regulated mass flow controllers. The flow lines from the vaporizer to the fuel-duct are heated to prevent condensation. The heating is controlled such that the temperature of the fuel stream at the fuel boundary is approximately 478 K. The velocities of the reactants at the boundaries are presumed to be equal to the ratio of their volumetric flowrates to the cross-section area of the ducts. Further details of the burner are given elsewhere [8,9].

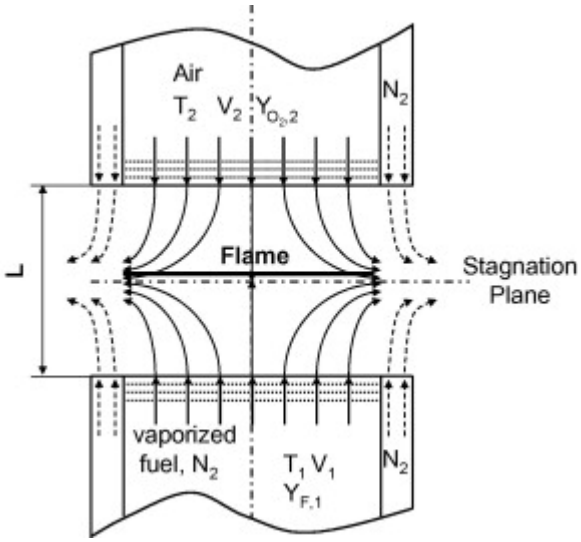

Figure 1. Schematic illustration of the counterflow flow field.

Figure 1 shows that the reactant streams flow toward a stagnation plane. The momentum of the two streams is approximately balanced to maintain the stagnation plane at the center of the two boundaries. Fine wire screens are placed at the exits of the fuel-duct and oxidizer-duct. This makes the tangential component of the flow velocity negligibly small at the exit of the ducts. The mass fraction of fuel, temperature, and component of the flow velocity normal to the stagnation plane at the fuel boundary are represented by $Y_{F,1}$, T_1, and V_1, respectively. The mass fraction of oxygen, temperature, and component of the flow velocity normal to the stagnation plane at the oxidizer boundary are represented by $Y_{O_2,2}$, T_2, and V_2, respectively. The distance between the fuel boundary and the oxidizer boundary is represented by L. Critical conditions of extinction are measured with L = 10 mm and ignition with L = 12 mm. The value of the strain rate, defined as the normal gradient of the normal component of the flow velocity, changes from the fuel boundary to the oxidizer boundary [10]. The characteristic strain rate on the air side of the stagnation plane a_2 is presumed to be given by [10]

$$a_2 = \frac{2|V_2|}{L}\left(1 + \frac{|V_1|\sqrt{\rho_1}}{|V_2|\sqrt{\rho_2}}\right) \quad (1)$$

Here ρ_1 and ρ_2 represent the density of the mixture at the fuel boundary and at the oxidizer boundary, respectively. Equation (1) is obtained from an asymptotic theory where the Reynolds numbers of the laminar flow at the boundaries are presumed to be large [10].

Critical conditions of extinction and ignition are measured that depend on the six experimental parameters of pressure, p, and the quantities a_2, $Y_{F,1}$, T_1, $Y_{O_2,2}$, and T_2. The experiments are carried out at atmospheric pressure. The oxidizer stream is air with $Y_{O_2,2}$ = 0.233. The temperature of the fuel stream, T_1 = 468 (±10) K. This fixes three of the six parameters. The extinction experiments are carried out with T_2 = 298 K. At some selected value of $Y_{F,1}$ the flame is stabilized at $a_2 < a_{2,e}$. The strain rate is increased by increasing V_1 and V_2 until extinction is observed. The strain rate at extinction, $a_{2,e}$, is recorded as a function of the mass fraction of fuel, $Y_{F,1}$. The accuracy of the strain rate is ±10% of recorded value and that of the fuel mass fraction ±3% of recorded value. The experimental repeatability on reported strain rate is ±5% of recorded value. The accuracy estimate is based on the accuracy of the flow-metering equipment used in the experiments. The experimental results are shown later.

The ignition experiments are carried out at fixed values of $Y_{F,1}$ = 0.4. The flow field is established at chosen values of strain rate. The temperature of air is increased until ignition takes place. The onset

of ignition is observed using a high-speed camera to make sure that ignition takes place close to the axis of symmetry. The temperature of the air stream, $T_{2,I}$ is recorded as a function of the strain rate, $a_{2,I}$. The accuracy of the measurement of the temperature of air at ignition is expected to be ±30 K, the strain rate ±10%, and fuel mass fraction ±3% of recorded value. The experimental repeatability in the measurement of the temperature of air at ignition is expected to be ±6 K. The accuracy of the temperature measurement is based on the accuracy of the radiation correction employed here to estimate the ignition temperature. The results are shown later.

3. Description of the chemical-kinetic mechanism

The detailed chemical kinetic model for methyl decanoate was recently developed by Herbinet et al. [7]. It is designed to simulate low-temperature chemistry including the negative temperature coefficient region. It also includes intermediate- and high-temperature chemistries. It has been validated by comparison of computed results to CFR engine experiments on methyl decanoate [5], to jet stirred reactor experiments on rapeseed methyl esters [4], and to shock tube experiments on *n*-decane [11,12]. In the paragraphs below, we give a short description of the model.

3.1. High-temperature part

At high temperatures, unimolecular decompositions of the fuel and H-atom abstractions from the fuel lead to the formation of alkyl and alkyl-ester radicals. Reactions of these radicals, which are known to be pertinent at high temperatures, are isomerizations, decompositions to olefins or unsaturated esters plus smaller radicals, and direct abstractions by O_2 to olefins or unsaturated esters plus HO_2. Olefins and unsaturated esters formed through these primary routes react in turn through the same types of reactions as the fuel and through other reactions specifically due the presence of the double bond (additions of radicals to the double bond, decomposition by retroene reactions).

H-atom abstractions from methyl decanoate by H, CH_3, C_2H_3, C_2H_5, O, O_2, OH, HO_2, CH_3O, and CH_3O_2 have been included. Distinctions between three types of H atoms were made: primary H atoms in the two methyl groups at each end of the molecule, secondary H atoms bonded to the conventional secondary, internal carbon atoms, and the two H atoms bonded to the carbon atom adjacent to the carbonyl group.

Alkyl and alkyl-ester radical decompositions were written in the reverse direction (addition of a radical to a double bond). Kinetic parameters are based on a recent review by Curran for the alkyl radicals [13] and from the methyl butanoate mechanism [2] for reactions involving atoms of the ester group. The kinetic parameters for addition of radicals to the oxygen of the C=O bond have been updated from the study of methyl radical addition to the C=O bond by Henry et al. [14]. Kinetic parameters used for isomerizations, or H-atom shifts, of radicals were taken from quantum calculations performed by Matheu et al. [15]. As far as olefins and unsaturated esters are concerned, rate constants for primary, secondary and tertiary H-atoms abstractions from olefins and unsaturated esters are the same as those described above for the methyl decanoate molecule.

3.2. Low-temperature part

The low-temperature part of the mechanism was built by adapting the kinetic scheme used in the well-validated *n*-heptane and *iso*-octane mechanisms. Again, some accommodations were required due to the presence of the methyl ester group in the fuel.

The first step of the low-temperature mechanism is the addition of alkyl and alkyl-ester radicals to O_2. The subsequent alkyl and alkyl-ester peroxy radicals (RO_2) react then by isomerizations to

hydroperoxy alkyl and hydroperoxy alkyl-ester radicals (QOOH). Isomerizations through 5, 6, 7 and 8 member cyclic transition states have been included.

Rate constants for QOOH decompositions to cyclic ethers plus OH and to olefin plus HO_2 are those recommended by Curran et al. [16]. Other reaction and rate constants in the low temperature part of the mechanism are not described here because they are not important under conditions studied here, but are described in [7].

The above described mechanism involves 3036 species and 8555 reactions. The large numbers of reactions and species are caused by the numerous types of reactions taken in account but also to the fact that methyl decanoate is not a symmetric molecule like an n-alkane. Isomerizations of RO_2 species in the low-temperature regime are also responsible for the large increase in the number of reactions because of the numerous permitted H-shifts.

3.3. Thermodynamic properties

Standard enthalpies of formation, entropies and specific heats of the molecules and radicals involved in the mechanism have been calculated using the THERM program developed by Ritter and Bozzelli [17]. This program is based on the group and bond additivity methods proposed by Benson [18].

The C-H bond dissociation energy of the carbon atom adjacent to the carbonyl group has been updated from the recent work of El-Nahas et al. [19] who studied the thermochemistry of methyl butanoate by performing quantum calculations. The value used in the mechanism for this specific bond is 94.1 kcal mol^{-1}. This compares closely to tertiary bond dissociation energies (96.5 kcal mol^{-1}) as noted above for H-atom abstractions from this site in methyl decanoate.

3.4. Transport properties

The transport parameters for the reduced mechanism presented in the next section were obtained from the CHEMKIN database [20], Marinov et al. [21], and using the critical temperature and pressure from the NIST WebBook [22] and the Tee, Gotoh, Stewart correlation as stated in [23]. The transport parameters for species for which critical properties were not available were estimated as being the same as other species similar in size and structure.

The entire mechanism, thermodynamic parameters and transport parameters are available in Ref. [24].

4. Mechanism reduction of methyl decanoate with directed relation graph

The detailed mechanism of methyl decanoate consists of 3036 species and 8555 reactions. Consequently computational simulation using this mechanism is very time consuming for zero-dimensional (0-D) simulations such as auto-ignition and perfectly stirred reactors (PSR), and is unaffordable for one-dimensional (1-D) simulations. Furthermore, it is even difficult to guess viable initial solutions for steady 1-D flows, such as premixed flames, to prevent the Newton solver from diverging with such a large mechanism. Therefore the detailed mechanism has to be reduced before being applied to diffusive systems. The major difficulty in its reduction is the large size. Since most conventional methods for mechanism reduction involve time consuming operations on sensitivity or Jacobian matrices, the reduction time of such methods typically scales as a cubic function of the size of the mechanism, and as such the reduction rapidly becomes unaffordable when the number of species becomes larger than a few hundreds. In the present study, the method of direct relation graph (DRG) [25-27] was selected to eliminate unimportant species and reactions from the detailed mechanism to obtain a skeletal mechanism that is sufficiently small for the simulation of counterflow

ignition. The method of DRG is based on linear-time operations [26], such that the reduction time scales linearly with the number of species. DRG can efficiently handle overly large mechanisms and is most suitable to apply as the first step in mechanism reduction to quickly bring down a large mechanism to a small size that can be further analyzed by other methods.

DRG quantifies species couplings with pair-wise reduction error in species production rates, which is defined in Ref. [25] as:

$$r_{AB} = \frac{\sum_{i=1,I}|\upsilon_{A,i}\omega_i\delta_{Bi}|}{\sum_{i=1,I}|\upsilon_{A,i}\omega_i|} \tag{2}$$

$$\delta_{Bi} = \begin{cases} 1 & \text{if the i}^{\text{th}}\text{ reaction involves species B} \\ 0 & \text{otherwise} \end{cases}$$

where the subscripts A and B indicate different species, i is the i^{th} reaction, $\upsilon_{A,i}$ the stoichiometric coefficient of species A in the i^{th} reaction, and ω the reaction rate. Each term on the denominator therefore indicates the contribution of the i^{th} reaction to the reaction rate of species A, and this term appears in the numerator only if the i^{th} reaction also involves species B. Since all the terms on the numerator are neglected if species B is eliminated, r_{AB} measures the relative error induced to species A due to the elimination of B. An error tolerance ϵ is then specified by the user, such that species B is considered important to A if

$$r_{AB} \geq \epsilon \tag{3}$$

That is, if species A is retained in the skeletal mechanism, B should also be retained. This requirement is expressed as A $\rightarrow$ B in graph notation. By further assuming the worst case error propagation within the graph, all the species required either directly or indirectly by species A are considered to be coupled with A. To resolve the species coupling with highest efficiency, a digraph, e.g. the DRG, is constructed based on the above graph notation. Species strongly coupled to the major species, such as the fuel and oxidizer, are subsequently identified through graph searching, and the set of skeletal species can be finally obtained. It is noted that DRG features a priori error control through the user-specified error tolerance, ϵ. More specifically, the worst case error of all the species in the skeletal mechanism is bounded by $O(\epsilon)$, such that no extensive validation is required for skeletal mechanisms obtained with DRG, provided the skeletal mechanism is applied within the parameter range of the reduction.

Nevertheless, it is seen that the DRG algorithm in Equations (2) and (3) is only for a single reaction state. To obtain a skeletal mechanism that is valid over a wide range of parameters, the DRG reduction can be performed on a set of reaction states sampled from representative applications, such as auto-ignition for ignition chemistry and PSR for steady burning and extinction. A species is retained in the final skeletal mechanism if it is required by any individual reaction state in the sample space. Comprehensive skeletal mechanisms can thereby be derived. In the present study, the sampled space consists of more than 3000 reaction states, densely covering the entire parameter range of interest, specifically atmospheric pressure, equivalence ratio from 0.5 to 1.5, initial temperature from 900 to 1300 K for ignition and 300 K for PSR, and N_2 diluted air with mole fraction for O_2 from 0.19 to 0.21. While the sampling process was performed in parallel on a 16-node PC cluster, taking about one day in wall clock time, the reduction based on the entire sample space took only about 20 min on a single 3 GHz P4 CPU.

Figure 2 shows the number of species in the resulting skeletal mechanisms as a function of the user-specified error tolerance. It is seen that the slope of the reduction curve is steep for small error tolerances, indicating that a large number of species can be eliminated with only minor induced

error. For example, a skeletal mechanism with 125 species and 713 elementary reactions was obtained with a reduction error of about 20%. This skeletal mechanism is sufficiently small and will be employed in the 1-D simulations of counterflow ignition and extinction in the following sections.

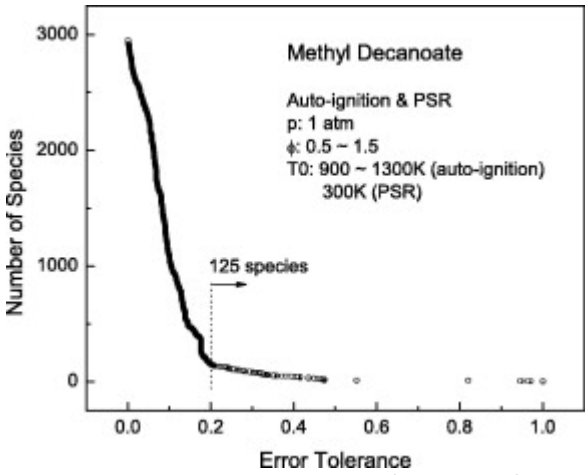

Figure 2. Number of species in skeletal mechanisms as a function of the threshold error specified in the reduction with directed relation graph, based on sampled reaction states from ignition and PSR.

The skeletal mechanism is validated in Figures 3 and 4 for auto-ignition and PSR, respectively, under selected conditions. Figure 3 shows the temperature profiles of stoichiometric methyl decanoate - air mixture under atmospheric pressure and different initial temperature. It is seen that the accuracy of the skeletal mechanism is better under the initial temperature of 1100 and 1300 K, while larger error occurs for 900 K. This indicates that the reaction pathways are more complex for ignition applications when the temperature is low. Validation for lean mixtures with equivalence ratio between 0.5 and 1 shows similar results. Figure 4 compares the skeletal mechanism with the detailed one in PSR. Fairly good accuracy can be observed. Larger error was observed for the PSR profiles with lower temperature, and the overall reduction error for PSR is smaller than that for ignition as shown in Figure 4. This indicates again the more complex reaction pathways at lower temperatures, as such the mechanism reduction for methyl decanoate was primarily constrained by the low-temperature chemistry.

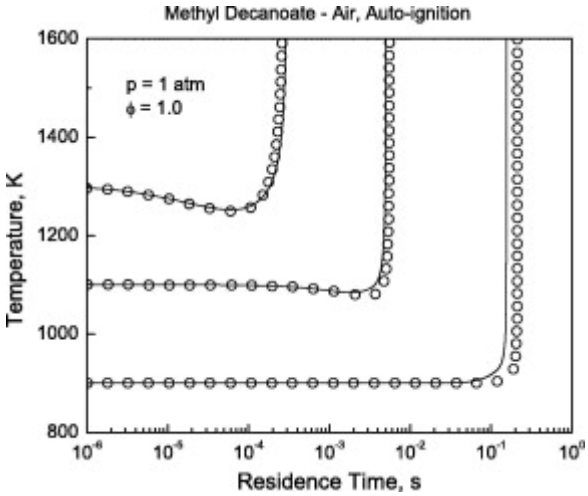

Figure 3. Temperature profiles for constant-pressure autoignition for stoichiometric methyl decanoate-air mixture under atmospheric pressure and at various initial temperatures, calculated with the detailed and 125-species skeletal mechanisms respectively. Lines: detailed, symbols: skeletal.

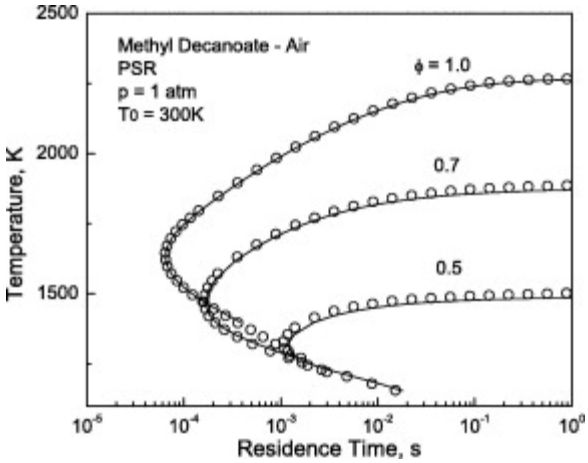

Figure 4. Dependence of temperature on residence time in PSR for methyl decanoate-air mixture with different equivalence ratio under STP, calculated with the detailed and 125-species skeletal mechanisms respectively. Lines: detailed, symbols: skeletal.

The skeletal chemical-kinetic mechanism is available in Ref. [24] and as Supplemental data.

5. Results and discussion

The skeletal mechanism was used to compute critical conditions of extinction and ignition, and the results were compared to the experiments. The computations were carried out using FlameMaster [28]. Plug flow boundary conditions were employed in the calculations. For a give composition and temperature of the reactant streams at the boundaries, the flow velocities V_1 and V_2 were increased until extinction takes place. The strain rate at extinction is calculated using Equation (1). Ignition calculations were performed by fixing the composition of the reactant streams, their flow velocities and the value of T_1, the temperature of air at the boundary, T_2 was increased until ignition took place. The strain rate at ignition is calculated using Equation (1). Figure 5 shows the mass fraction of fuel, $Y_{F,1}$, as a function of the strain rate at extinction, $a_{2,e}$. The symbols in this figure represent experimental data and the line results of calculations. They separate a flammable region for $a_2 < a_{2,e}$ from a nonflammable region for $a_2 > a_{2,e}$. At a give value of strain rate the calculated fuel mass fraction at extinction is lower than the measured value. Figure 6 shows the temperature of air at ignition, $T_{2,I}$, as a function of the strain rate, a_2 for fixed values of $Y_{F,1}$ = 0.4. The symbols represent experimental data. The line in Figure 6 represents results of numerical calculations using the skeletal mechanism. It separates a region for $T_2 > T_{2,I}$ where ignition can take place from a region where ignition is not possible. For a given a_2 the calculated value of $T_{2,I}$ is higher than the measured value. The agreement between numerical calculations and experimental data for extinction and ignition is considered to be reasonably good.

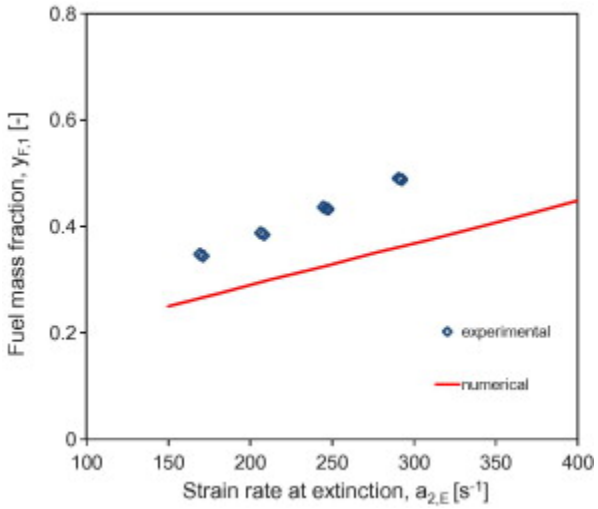

Figure 5. The mass fraction of fuel, $Y_{F,1}$, as a function of the strain rate at extinction, $a_{2,e}$. The symbols represent experimental data. The line is results of numerical calculation using the skeletal mechanism.

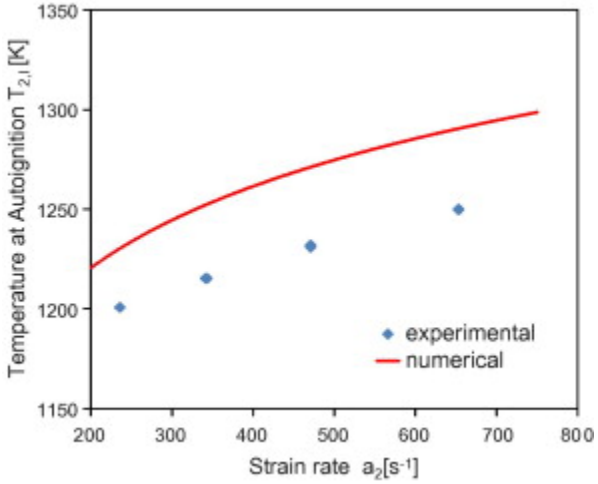

Figure 6. The temperature of the oxidizer stream at ignition, $T_{2,I}$, as a function of the strain rate, a_2 for $Y_{F,1}$ = 0.4. The symbols represent experimental data. The line is result of numerical calculations using the skeletal mechanism.

In the reduction process, calculations of 0-D ignition states and 0-D PSR states were used to determine the chemistry important for ignition and extinction in the counterflow system. One of the most interesting features is that the low-temperature chemistry was found to be of little importance under these counter flow conditions. Only 23 reactions of the original set of over 4000 low-temperature reactions were retained after reduction. These reactions are shown in Table 1 and have been grouped according to their unique characters. The first group (group 1) corresponds to reactions involving the methylperoxy radicals. These reactions either lead to the production of reactive radials like methoxy or to chain termination. An example of the former is $CH_3O_2 + CH_3O_2 \rightleftharpoons O_2 + CH_3O + CH_3O$ which converts two reactively unreactive methyl peroxy radicals into two reactive methoxy radicals. An example of chain termination is $CH_3O_2 + CH_3O_2 \rightleftharpoons CH_2O + CH_3OH + O_2$ which converts two methylperoxy radicals into two stable products. The next group (group 2) consists of radical addition to O_2 that can again lead to either reactive or unreactive products. The reactive paths lead to the OH radical, the main chain carrying radical under low-temperature conditions. The other paths lead to unreactive products consisting of olefins and HO_2 radicals. The reduction process indicates that it is important to retain the balance between unreactive and reactive products represented in groups 1 and 2 in order to properly predict ignition and extinction processes. It is also

interesting to note that all the reactions involving methyl esters involve the number 2 site (the carbon next to the carbonyl group) or the methyl site (on the ester group). These two sites allow a fast 6-member ring isomerization of the type RO_2 to QOOH which leads to reactive OH radicals and acceleration of the overall reaction rate. The final group in Table 1 is group 3 which has a different character and consists only of reactions involving radical addition to O_2 to form alkylperoxy radicals. The subsequent reactions to consume the alkylperoxy radicals have been eliminated in the mechanism reduction process. This indicates that radicals, R, are generated and then added to O_2 to form alkylperoxy radicals which act as a temporary reservoir for the R radicals. This reservoir is depleted as the temperature is increased during the ignition process when the $R + O_2 \rightleftharpoons RO_2$ reaction reverses itself to give back the R radical.

Table 1. Low-temperature reactions retained in reduced mechanism

Reaction group 1:
$CH_3 + O_2 \leftrightharpoons CH_3O_2$
$CH_3O_2 + CH_3 \leftrightharpoons CH_3O + CH_3O$
$CH_3O_2 + CH_3O_2 \leftrightharpoons CH_2O + CH_3OH + O_2$
$CH_3O_2 + CH_3O_2 \leftrightharpoons O_2 + CH_3O + CH_3O$
$CH_3O_2 + OH \leftrightharpoons CH_3OH + O_2$
$C_3H_5\text{-}A + CH_3O_2 \leftrightharpoons C_3H_5O + CH_3O$
Reaction group 2:
$C_2H_5 + O_2 \leftrightharpoons C_2H_5O_2$
$C_2H_5O_2 \leftrightharpoons C_2H_4 + HO_2$
$NC_3H_7 + O_2 \leftrightharpoons NC_3H_7O_2$
$NC_3H_7O_2 \leftrightharpoons C_3H_6OOH1\text{-}2$
$C_3H_6 + HO_2 \leftrightharpoons C_3H_6OOH1\text{-}2$
$C_3H_6OOH1\text{-}2 \leftrightharpoons C_2H_4 + CH_2O + OH$
$NC_3H_7O_2 \leftrightharpoons C_3H_6 + HO_2$
$MPMJ + O_2 \leftrightharpoons MPMO_2$
$ME2J + O_2 \leftrightharpoons ME_2O_2$
$MEMO_2 \leftrightharpoons MEMOOH_2J$
$MPMO_2 \leftrightharpoons MPMOOH_2J$
$MEMOOH\text{-}2J \leftrightharpoons MEOM\text{-}2 + OH$
$MPMOOH2J \leftrightharpoons MPOM\text{-}2 + OH$
Reaction group 3:
$MEMJ + O_2 \leftrightharpoons MEMO_2$
$C_8H_{17}\text{-}1 + O_2 \leftrightharpoons C_8H_{17}O_2\text{-}1$
$C_7H_{15}\text{-}1 + O_2 \leftrightharpoons C_7H_{15}O_2\text{-}1$
$MD2J + O_2 \leftrightharpoons MD2O_2$

Notation: MD, methyl decanote; ME, methyl ethanoate; MP, methyl propanoate. Numbers on methyl ester structures refer to carbon position relative to carbonyl carbon which is position 1.

On the other hand, the chemistry retained by the reduction process was the fuel decomposition reactions, and the abstraction of H atoms from the fuel by OH, H, O, HO_2, CH_3, CH_3O, C_2H_3, C_2H_5, and O_2. After the fuel reactions, the following subsequent reactions were retained: the decomposition of fuel radicals, reaction of fuel radicals with O_2 to form olefins, and isomerization of fuel radicals. The main intermediates species with ester moieties that were also kept had olefinic structures: methyl butenoate and methyl propenoate. These olefin-methyl ester structures are derived from the decomposition of the methyl decanoate radicals and their decomposition products. Comparing

methyl ester fuels with alkane fuels, these intermediates correspond to olefins like butene and propene derived from alkane fuels. The formation of these olefins with methyl ester moieties is consistent with the experimental observations of Dagaut et. al. [29]. We did not make direct comparisons with their data set because the fuel studied consisted of rapeseed methyl esters and kerosene. The reduced model is not capable of simulating kerosene.

6. Concluding remarks

The DRG method is a very powerful technique that could be employed to simplify detailed mechanism. It was used here to obtain a skeletal mechanism for describing combustion of methyl decanoate from a detailed mechanism. Simulations of ignition in 0-D systems and of steady burning and extinction in PSR carried out using the skeletal mechanism agree well with those calculated using the detailed mechanism. Predictions of extinction and ignition of methyl decanoate in non-premixed flows obtained using the skeletal mechanism agree well with the experimental data. The derived skeletal mechanism shows that low-temperature chemistry is of minor importance under the counterflow conditions considered. The reaction chemistry of most importance are the high-temperature reactions of fuel decomposition, radical abstraction, isomerization, and radical decomposition. Formation and consumption of olefin intermediates with ester moieties were also found to be significant.

Acknowledgment

The research at the University of California at San Diego is supported by UC Discovery/Westbiofuels, Grant # GCP06-10228. The work at Princeton University was supported by the Air Force Office of Scientific Research under the technical monitoring of Dr. Julian M. Tishkoff, and a block grant awarded by BP and Ford on carbon mitigation. The work at LLNL was supported by the US Department of Energy, Office of the Freedom CAR and Vehicle Technologies, program manager Kevin Stork and Gurpreet Singh, and performed under the auspices of the US Department of Energy by Lawrence Livermore National Laboratory under Contract DE-AC52-07NA27344.

Supplementary material

Detailed kinetic model separated in three files (mechanism, thermodynamic properties and transport data).

References

[1] S. Gaïl, M. Thomson, S. Sarathy et al., Proc. Combust. Inst., 31 (2007), pp. 305–311

[2] E.M. Fisher, W.J. Pitz, H.J. Curran, C.K. Westbrook, Proc. Combust. Inst., 28 (2000), pp. 1579–1586

[3] S. Sarathy, S. Gaïl, S. Syed, M. Thomson, P. Dagaut, Proc. Combust. Inst., 31 (2007), pp. 1015–1022

[4] P. Dagaut, S. Gaïl, M. Sahasrabudhe, Proc. Combust. Inst., 31 (2007), pp. 2955–2961

[5] J.P. Szybist, A.L. Boehman, D.C. Haworth, H. Korga, Combust. Flame, 149 (2007), pp. 112–128

[6] J.A. Szybist, J. Song, M. Alam, A.L. Boehman, Fuel Process. Technol., 88 (2007), pp. 679–691

[7] O. Herbinet, W.J. Pitz, C.K. Westbrook, Combust. Flame, 154 (3) (2008), pp. 507–528

[8] R. Seiser, L. Truett, D. Trees, K. Seshadri, Proc. Combust. Inst., 27 (1998), pp. 649–657

[9] R. Seiser, K. Seshadri, E. Piskernik, A. Liñán, Combust. Flame, 122 (2000), pp. 339–349

[10] K. Seshadri, F.A. Williams, Int. J. Heat Mass Transfer, 21 (2) (1978), pp. 251–253

[11] D. Davidson, J. Herbon, D. Horning, R. Hanson, Int. J. Chem. Kinet., 33 (12) (2001), pp. 775–783

[12] U. Pfahl, K. Fieweger, G. Adomeit, Proc. Combust. Inst., 26 (1996), pp. 781–789

[13] H.J. Curran, Int. J. Chem. Kinet., 38 (4) (2006), pp. 250–275

[14] D.J. Henry, M.L. Coote, R. Gomez-Balderas, L. Radom, J. Am. Chem. Soc., 126 (6) (2004), pp. 1732–1740

[15] D.M. Matheu, W.H. Green, J.M. Grenda, Int. J. Chem. Kinet., 35 (3) (2003), pp. 95–119

[16] H.J. Curran, P. Gaffuri, W.J. Pitz, C.K. Westbrook, Combust. Flame, 129 (2002), pp. 253–280

[17] E.R. Ritter, J.W. Bozzelli, Int. J. Chem. Kinet., 23 (9) (1991), pp. 767–778

[18] S.W. Benson, Thermochem. Kinet., (second ed.)John Wiley, New York (1976)

[19] A.M. El-Nahas, M.V. Navarro, J.M. Simmie et al., J. Phys. Chem. A, 111 (19) (2007), pp. 3727–3739

[20] R.J. Kee, J. Warnatz, J.A. Miller, A Fortran Computer Code Package for the Evaluation of Gas Phase Viscosities, Conductivities and Diffusion Coefficients, Tech. Rep. SAND83-8209, Sandia National Laboratories, Livermore, CA, 1983.

[21] N.M. Marinov, W.J. Pitz, C.K. Westbrook, A.E. Lutz, A.M. Vincitore, S.M. Senkan, Proc. Combust. Inst., 27 (1998), pp. 605–613

[22] NIST Standard Reference Database Number 69, NIST Chemistry WebBook, 2003.

[23] L.S. Tee, S. Gotoh, W.E. Stewart, Ind. Eng. Chem., 5 (3) (1966), pp. 356–363

[24] Available at http://www-cmls.llnl.gov/?url=science_and_technology-chemistry-combustion.

[25] T.F. Lu, C.K. Law, Proc. Combust. Inst., 30 (2005), pp. 1333–1341

[26] T.F. Lu, C.K. Law, Combust. Flame, 144 (2006), pp. 24–36

[27] T.F. Lu, C.K. Law, Combust. Flame, 146 (2006), pp. 472–483

[28] H. Pitsch, FlameMaster, A C++ Computer Program for 0D Combustion and 1D Laminar Flame Calculations, Tech. rep., Institut für Technische Mechanik, RWTH Aachen, may be downloaded from available at http://www.stanford.edu.bases-doc.univ-lorraine.fr/group/pitsch/CES.htm.

[29] P. Dagaut, S. Gaïl, J. Phys. Chem. A, 111 (19) (2007), pp. 3992–4000